Real-time activity of dynorphin-expressing neurons in mouse central amygdala during alcohol drinking

Abbreviated Title (50 character max): Dynorphinergic CeA neurons' activity in alcohol drinking

Christina L. Lebonville[1,2], Jennifer A. Rinker[1,2], Krysten O'Hara[1,2], Christopher S. McMahan[3], Michaela Hoffman[2], Howard C. Becker[2], Patrick J. Mulholland[1,2]

[1]Department of Neuroscience, Charleston Alcohol Research Center, Medical University of South Carolina, Charleston SC, 29425

[2]Department of Psychiatry & Behavioral Sciences, Charleston Alcohol Research Center, Medical University of South Carolina, Charleston SC, 29425

[3]School of Mathematical and Statistical Sciences, Clemson-MUSC Artificial Intelligence Hub, Clemson University, Clemson, SC 29634-0975

Corresponding author: Patrick J. Mulholland
mulholl@musc.edu

Conflict of Interest: The authors declare no competing financial interests.

Funding & Acknowledgements*:* These studies were financially supported by the Charleston Alcohol Research Center (P50 AA010761), the INIAstress Consortium (U01 AA014095, U01 AA020930), VA Medical Research (BX000813, HCB), and NIH grants F32 AA029026 (CLL), OD021532 (PJM), AA023288 (PJM), AA02653 (HCB), and K01 AA025110 (JAR).

Abstract

Alcohol use disorder (AUD) is a prevalent chronic relapsing disease, affecting 30 million people (10.5%) in the United States alone that poses significant economic burden and health risks. Evidence from human and animal studies has identified crucial brain regions that are important for driving binge alcohol (ethanol) drinking and excessive drinking produced by the development of AUD. In preclinical models, the central amygdala (CeA) has emerged as a key mediator of binge alcohol consumption. A dynorphin-expressing subpopulation within the CeA (CeA^{Dyn}) has been implicated in excessive alcohol drinking across both acute and chronic alcohol exposure models. Yet, how cellular activity of CeA^{Dyn} neurons is impacted by active alcohol drinking is not well-understood. Thus, it is pivotal to better understand specific brain mechanisms underlying the behavioral and physiological responses to alcohol that promote alcohol misuse. The goal of the current study was to probe the engagement of CeA^{Dyn} neurons in male and female mice during voluntary alcohol consumption using fiber photometry and to compare alcohol phenotypes with that of water and sucrose. Activity of the Cre-dependent calcium sensor, GCaMP7f, in the CeA of prodynorphin-Cre (Pdyn-Cre) mice was recorded and time-locked to bouts of licking during 2-hr, 20% alcohol drinking. To rigorously analyze this photometry data, multilevel modeling protocols were applied to better understand sex and temporal effects in these complex time series data. Analysis revealed a large increase in CeA^{Dyn} neuron calcium transients after bouts of licking for alcohol, and only modest increases during licking for water or 0.5% sucrose, indicating these neurons are uniquely engaged during alcohol consumption. Further testing revealed that differences in drinking behavior unique to alcohol (i.e. longer bout durations) do not fully explain signal differences between alcohol and other solutions nor is the alcohol response diminished across the 2-hr drinking session. These findings identified a unique functional signature for alcohol in a cell population that is known to control binge alcohol drinking.

Introduction

Alcohol use disorder (AUD) is a prevalent chronic relapsing disease, affecting 30 million people (10.5%) in the United States alone (SAMHSA 2022) and poses significant negative economic and health consequences (Sacks et al 2015, WHO 2018). Evidence from human and animal studies has revealed brain regions involved in excessive alcohol drinking and the development of AUD, including the amygdala (for review: Roberto et al 2020). In rodent models of excessive alcohol (ethanol) drinking, the extended amygdala has emerged as a key mediator of alcohol consumption, particularly in alcohol dependence. A dynorphin-expressing subpopulation within the central amygdala (CeA^{Dyn}) has been implicated in excessive alcohol drinking across both acute and chronic alcohol exposure models (for review: Walker et al 2021). Yet, how cellular activity of CeA^{Dyn} neurons is impacted by active alcohol drinking is not well-understood. Thus, it is pivotal to better understand specific brain mechanisms underlying the behavioral and physiological responses to alcohol that promote alcohol misuse.

The amygdala complex itself is a complex structure of five major subdivisions and up to 13 different sub-nuclei. The central amygdala (CeA) has three sub-nuclei comprised of heterogeneous GABAergic neurons that express different neuropeptides. Of the diverse neuropeptide populations in the CeA, dynorphin-expressing CeA neurons (CeA^{Dyn}) are known to regulate both binge alcohol drinking and stress-enhanced drinking in alcohol dependence (Anderson et al 2019, Haun et al 2022, Bloodgood et al 2020). CeA^{Dyn} signaling disruption influences alcohol drinking in a sex-dependent manner and, similarly, prolonged alcohol exposure increases excitability of CeA^{Dyn} neurons in male, but not female mice (Bloodgood et al 2020). How real-time activity of CeA^{Dyn} neurons relates to alcohol drinking is not well explored, nor is it clear why alcohol exposure would differentially affect male and female CeA^{Dyn} activity. The current studies were designed to investigate CeA^{Dyn} neuron activity dynamics relative to alcohol drinking, whether these effects differ depending on biological sex, and whether consumption of other solutions also similarly engage CeA^{Dyn} neurons.

To capture real-time activity of CeA^{Dyn} neurons during voluntary consumption of alcohol, water, and sucrose, we used in vivo fiber photometry in freely behaving male and female (pro)Dyn-Cre mice. Because of the complex structure of time series data using a within-subjects experimental design, such as that acquired in this fiber photometry drinking study, a multilevel linear mixed model (MLMM) approach offers notable advantages (see Gueorguieva and Krystal 2004 for comparison). Specifically, MLMMs are designed to account for data that exist in a nested, repeated measures structure, even with missing data or unbalanced designs (West et al 2022). Compared to repeated measures or nested ANOVAs that consider random variation from a single source (usually within subject), MLMMs can better estimate composite effects of multiple random variables from a complex, nested data structure, providing more power to detect and accurately estimate effects from critical variables (see Aarts et al 2014). This is relevant to the current study in that mice showed individual variation within and across drinking sessions and solutions. For this study, MLMMs provide a statistically sound foundation for testing both primary and secondary hypotheses on the relationship between alcohol drinking and CeA^{Dyn} neuron calcium activity. We hypothesized that CeA^{Dyn} neurons would show distinct signaling for alcohol drinking compared to these other substances, given the substantial evidence of this population's importance to alcohol consumption and dependence, and that males would show a more pronounced pattern of activity compared to females, due to reported sex differences in the engagement of CeA^{Dyn} neurons. Collectively, these studies aimed to understand early alcohol engagement of CeA^{Dyn} neurons in both sexes to better understand the role of these responses in promoting binge alcohol drinking.

Methods

Animals: Male and female prodynorphin-Cre (proDyn-Cre) mice (n = 26, 13 male, 13 female) were bred in-house from homozygous Pdyn-Cre mice (expressing Cre-recombinase in cells positive for dynorphin-precursor, *Pdyn*) and C57BL/6J mice procured from Jackson Laboratory (B6;129S-$Pdyn^{tm1.1(cre)Mjkr}$/LowlJ, JAX Stock #027958 and C57BL/6J, JAX Stock #000664). Mice were 8-13 weeks of age at the start of the experiments and allowed *ad libitum* access to food throughout and water outside of experimental 2-hr sessions. Mice were individually housed on a reversed 12-hr light-dark cycle (lights off at 9 am). All animal procedures were approved and facilities inspected by the Medical University of South Carolina's (MUSC) Institutional Animal Care and Use Committee (IACUC). MUSC is accredited by the Association for the Assessment and Accreditation of Laboratory Animal Care (AAALAC) and meets U.S. Department of Agriculture and Public Health Service standards and regulations. Mice were run in two independent, mixed-sex cohorts. Any mice that did not show spontaneous

acute GCaMP7f activity were removed at the onset of the study while any mice determined to have off target ferrule or viral placement were removed from the final analysis after histological verification.

Surgery & Viruses: Mice underwent unilateral surgical delivery of a Cre-dependent GCaMP7f calcium sensor into the CeA (pGP-AAV1-syn-FLEX-jGCaMP7f-WPRE, a gift from Douglas Kim & GENIE Project, Addgene viral prep # 104492-AAV1; http://n2t.net/addgene:104492; RRID:Addgene_104492, Lots v49556 and v118530 with titers of 1-2 x10^{13} GC/mL) and implantation of a fiber optic ferrule (MFC_400/430-0.57(or 0.66)_5.3mm_ZF2.5(G)_FLT, Doric Lenses Inc, Quebec, QC, Canada) above the target CeA population. The virus was delivered at a volume of 200 nL and rate of 100 nL/min. Following infusion, injectors remained in place for 10 min to allow for diffusion away from the injector tip before injector retraction. Target stereotaxic coordinates for CeA were -1.4 AP, +2.7 ML, -4.7 virus/-4.62 fiber DV (in mm relative to bregma) based on the mouse stereotaxic atlas (Franklin and Paxinos 2008). Mice were administered carprofen (5 mg/kg, IP), xylocaine (2%, topical), and bacitracin/polymixin (2%, topical) at the time of surgery and carprofen (5 mg/kg, SC) xylocaine (2%, topical), and bacitracin/polymixin (2%, topical) for post-surgery recovery for at least 2 days. Mice were then given at least 5 weeks to recover from surgery and for viral incubation before being acclimated to tethering procedures and testing GCaMP7f signal.

***Binge Access to Alcohol*:** Mice were given access to a single bottle of 20% (v/v) alcohol 3 hours into the dark cycle in their home cages for 2 hours/day, 5 days/week for 3 consecutive weeks. Mice were then given access to a single bottle of water in the same manner for two weeks and then a single bottle of 0.5% sucrose (w/v) for three weeks. Identical graduated sipper tubes were used for all three solutions. To confirm that sipper tube contacts were licking bouts, we trained a deep-learning model using DeepEthogram (Bohnslav et al 2021) on overhead video recordings of drinking sessions with 95% average accuracy compared to manual experimenter validation.

Fiber Photometry Recording and Processing: Fiber optic patch cords containing rotary joints (Doric; 0.57 NA; 400 µm) were mounted within custom-built balance arms to allow free exploration and head movement. Patch cord terminals were connected to sterilized chronic indwelling optic fiber cannula (Doric; 0.57-0.66 NA) using pinch connectors (Thorlabs Inc., Newton, NJ, USA). After habituating mice to tethering procedures, CeA^{Dyn+} neuronal calcium transients were recorded from two mice during each drinking session. Consecutive recording sessions were limited to two days to prevent possible GCaMP7f photobleaching. During recording, GCaMP7f was excited using a collimated 470 nm LED (Thorlabs), and signal from a concurrent 405 nm LED was used for normalization to control for movement artifacts. Illumination power for each LED (5-30 µW) was sinusoidally modulated at 531 Hz (405 nm) and 211 Hz (470 nm) and was passed through Doric fluorescent Mini Cubes. Emission light was focused onto a femtowatt photoreceiver (Newport, model 1672151; DC low setting) and sampled at 6.1 kHz by a RZ5P lock-in digital processor controlled by photometry processing software (Synapse, Tucker-Davis Technologies, Alachua, FL, USA). The GCaMP7f signal was integrated in real-time with licking behavior for alcohol, water, and sucrose in sipper tubes using lickometer circuits (Med Associates Inc., Fairfax, VT, USA) following our previous methods (Rinker et al 2018). Fiber optic patch cords were photobleached twice weekly overnight using a 405 nm LED to reduce autofluorescence. Raw, demodulated emission signals were normalized and processed using custom MATLAB scripts according to our standard protocol (Rinker et al preprint). Briefly, %d*F*/*F* = [(detrended 470 nm signal - detrended and corrected 405 nm signal)/detrended and corrected 405 nm signal]*100. After extracting mean signal 1 sec before and after a drinking bout, we then standardized each signal within-mouse by subtracting the mouse-specific experiment-wide mean signal from each value and dividing each resulting value by the mouse-specific experiment-wide standard deviation to produce a z-score, standardized within-mouse (z%d*F*/*F*). Licking behavior was identified as a bout if lick frequency was >4.5 Hz, interlick interval was <500 ms, and duration was >500 ms based on the known microstructure of rodent drinking behavior (Davis 1992; Boughter 2007; Johnson 2010).

Machine Learning Pipeline for 405 nm Correction: The goal of our novel machine learning pipeline was to correct Ca^{2+}-dependent deflections in the 405 signal during periods of high signal in the 470 nm channel. To this end, we conceptualize a model for the 470 series, $\{y_t\}_{t=1}^{T}$, and the 405 series, $\{x_t\}_{t=1}^{T}$, that is given by

$$y_t = \beta_0 + \beta_1 + f(t) + \varepsilon_t, \quad (1)$$
$$x_t = \alpha_0 + \alpha_1 + g(t) + \delta_t, \quad (2)$$

where β_0 (α_0) is the usual intercept, $\beta_1(\alpha_1)$ is a slope parameter that capture the general trend of the series, f (g) is a time dependent function that captures the fluctuation around the general trend, and ε_t (δ_t) is a random error term. To provide a flexible specification, we make use of B-splines to model f and g; i.e., we specify

$$f(t) = \sum_{l=1}^{L} b_l(t)\gamma_l^f,$$
$$g(t) = \sum_{l=1}^{L} b_l(t)\gamma_l^g,$$

where $\gamma_l^f(\gamma_l^g)$ are spline coefficients that are unique to f (g) and $b_l(t)$ are B-spline basis functions which are fully determined once a knot set and degree are specified. In our implementation, we make use of a knot set consisting of 147 interior knots placed at equally spaced quantiles of the series and specify the degree to be 3, this yields 150 basis functions; for further discussion on B-splines and their uses, see (de Boor 1972). Our use of B-splines in this context affords us a two primary benefits. First, our specifications allow for a great deal of modeling flexibility rendering our model more than adept at capturing fluctuations around the trend. However, this flexibility comes at the expense of potential overfitting issues. To mitigate this potential, we regularize the estimation of the spline coefficients via the following penalty

$$J_1^f(\boldsymbol{\gamma}^f) = \boldsymbol{\gamma}^{f'}\boldsymbol{D}'\boldsymbol{D}\boldsymbol{\gamma}^f,$$
$$J_1^g(\boldsymbol{\gamma}^g) = \boldsymbol{\gamma}^{g'}\boldsymbol{D}'\boldsymbol{D}\boldsymbol{\gamma}^g,$$

where $\boldsymbol{\gamma}^f = (\gamma_1^f, \dots, \gamma_L^f)'$, $\boldsymbol{\gamma}^g = (\gamma_1^g, \dots, \gamma_L^g)'$ and $\boldsymbol{D}$ is a $(L-1) \times L-$ dimensional first order difference matrix; i.e., $\boldsymbol{D}_{ll} = 1$ and $\boldsymbol{D}_{l,l+1} = -1$, for $l = 1, \dots, L-1$, and $\boldsymbol{D}_{lk} = 0$ otherwise, for further discussion see (Eilers and Marx 1996). The second benefit of this specification, is it affords us the ability to enforce functional similarity between f and g through the following penalty

$$J(\boldsymbol{\gamma}) = \int_0^T \{f(t) - g(t)\}\text{^}2dt,$$

where $\boldsymbol{\gamma} = (\boldsymbol{\gamma}^f, \boldsymbol{\gamma}^g)'$**.** Leveraging the spline representation, this penalty can be expressed in matrix form as follows $J(\boldsymbol{\gamma}) = \boldsymbol{\gamma}'\boldsymbol{J}\,\boldsymbol{\gamma}$, where

$$\boldsymbol{J} = \begin{bmatrix} \boldsymbol{J}^* & \boldsymbol{J}^* \\ \boldsymbol{J}^* & \boldsymbol{J}^* \end{bmatrix},$$

and $\boldsymbol{J}_{ll'}^* = \int_{\boldsymbol{0}}^{\boldsymbol{T}} b_l(t)b_{l'}(t)dt$**.** Finally, the last regularization term that we adopt is a ridge penalty that acts to shrink regression coefficients toward 0; i.e., we specify the following penalty

$$J_R(\boldsymbol{\gamma}) = \sum_{l=1}^{L}\left(\gamma_l^f\right)^2 + \sum_{l=1}^{L}\left(\gamma_l^g\right)^2.$$

Thus, the objective function used to fit (1) and (2) is given by

$$L(\boldsymbol{\alpha}, \boldsymbol{\beta}, \boldsymbol{\gamma}) = \sum_{t=1}^{T}\left(y_t - \beta_0 - \beta_1 t - \sum_{l=1}^{L} b_l(t)\gamma_l^f\right)^2 + \sum_{t=1}^{T}\left(x_t - \alpha_0 - \alpha_1 t - \sum_{l=1}^{L} b_l(t)\gamma_l^g\right)^2 + J^*(\boldsymbol{\gamma};\ \lambda_1, \lambda_2, \lambda_3),$$

where $J^*(\boldsymbol{\gamma};\ \lambda_1, \lambda_2, \lambda_3) = \lambda_1 J(\boldsymbol{\gamma}) + \lambda_2 J_R(\boldsymbol{\gamma}) + \lambda_3 J_1^f(\boldsymbol{\gamma}^f) + \lambda_3 J_1^g(\boldsymbol{\gamma}^g)$, $\boldsymbol{\alpha} = (\alpha_0, \alpha_1)'$, and $\boldsymbol{\beta} = (\beta_0, \beta_1)'$. A few comments are warranted. First, the minimizer of the aforementioned objective function can be computed in closed form for any value of the penalty parameters λ_1, λ_2, and λ_3. Second, different configurations of the penalty

parameters ultimately yield different model fits. To select the best set, we utilize the BIC criterion with the degrees of freedom being computed as the trace of the smoothing matrix (for further discussion of this strategy see Hastie et al 2009). Given the parameter estimates arising from this process, we make use of the fitted values to correct the detrended 405 nm signal.

Histological Validation: After behavioral experiments, mice were sacrificed by injection with 50% urethane and, at surgical anesthetic depth, transcardial perfusion with 1X phosphate buffered saline (PBS) and 4% paraformaldehyde solution. Brains were extracted and stored in 4% paraformaldehyde solution until further processing. Brains were sliced into 40 µm thick sections on a vibratome (VT100S, Leica Microsystems, Wetzlar, Germany) which were then slide mounted to charged glass slides and coverslipped using VECTASHIELD Vibrance® with DAPI (Vector Labs, Burlingame, CA, USA) or ProLong™ Glass with NucBlue™ (Thermo Fisher Scientific, Waltham, MA, USA). On-target and dorsal placement of the fiber ferrule above GCaMP7f expression was visually verified using a fluorescent microscope (EVOS fl, AMG, Bothell, Washington, USA). Representative images were captured using a confocal microscope (Carl Zeiss LSM 880, Oberkochen, Germany).

Statistical Analysis and Multilevel Linear Mixed Modelling: Our "base" model included the primary factors of interest (i.e. Sex, Solution, and time around bout) as fixed (independent) variables. To determine how these primary variables of interest were related independently to calcium signal or to various drinking characteristics, we included signal or characteristic as a single outcome variable for this base model ("outcome model") and empirically tested various random effects structures for each outcome using an unconditional means model (absent any fixed variables). We selected the random effects that were logical given the data structure, were appropriately levelled for the outcome, and gave the highest ICC and lowest AIC/BIC. For all models, centered orthogonal contrasts (Helmert) were used for categorical variables (i.e. Sex, Time, Solution) to reduce problems with variance estimation (Yaremych et al 2021). To test hypotheses about the relationship between signal and drinking characteristics, we added each variable as a fixed independent factor in the "signal-outcome" model to generate a "signal-characteristic" model. To avoid estimation bias in upper-level interaction effects and to increase interpretability, scaled mean-centered forms of independent variables were used. When levels of a variable are described as "high" or "low", this refers to estimates at -1 or +1 standard deviation from the mean, respectively. All tests were performed in R with custom scripts (available upon request) using the "lme4" package (Bates et al 2015) and guidance from West et al 2022.

Results

Final Dataset & Models

The experimental design of the current studies is described in **Figure 1A**. Of the 26 (13 female/13 male) pro(Dyn)-Cre mice who underwent surgery to express GCaMP7f in the CeA, one female and one male mice were lost due to surgical complications and six female and two male mice were removed early from the experiments due to having low spontaneous calcium signal. Following experimentation, we histologically validated GCaMP7f expression and fiber placement within the CeA (**Figure 1C)** and removal two males for nonspecific virus expression. Validation of drinking bouts using the trained DeepEthogram model led to removal of only 11% of all bouts and 14/136 sessions due to having no drinking bouts or being technically unable to validate bouts (i.e. room red light was off). The final dataset included calcium and drinking data from n = 14 mice (8 male, 6 female) over 122 sessions, and 2832 drinking bouts. To account for random differences between repeated sessions and bouts within mice and provide better statistical power to test relationships between the primary factors of interest, we employed a

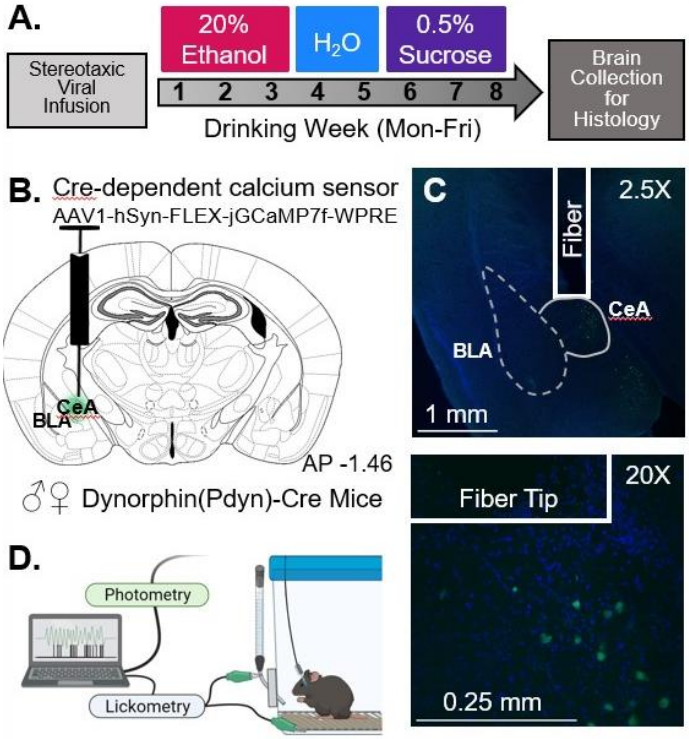

FIGURE 1. Experimental timeline (**A**). Strategy for viral infusion of Cre-dependent GCaMP7f into the CeA (**B**) and fiber optic ferrule implantation above injection site to record from CeA^{Dyn+} neurons. Representative images of viral expression and fiber optic ferrule placement at 2.5X and 20X magnification (**C**). Home cage drinking with lickometry and photometry set-up (**D**).

MLMM approach with random slopes and intercepts (see **Table 1**). We employed different MLMMs depending on the hypothesis being tested and the random effect structure was optimized for each outcome variable. To test hypotheses on the relationship between bout characteristics (bout duration and temporal occurrence within a session) and calcium signal, we added fixed variables to the signal-outcome model that pertained to specific hypotheses ("signal-characteristics model"). The experimental data structure is presented in **Figure 2**.

Table 1. Multilevel Linear Mixed Model (MLMM) Design

Level	Fixed Variables (**Bold** = Primary Interests, "Base Model")	Random Variables	Outcome Variables
Mouse (Lvl 4)	**Time** (Lvl 1), **Solution** (Lvl 3), **Sex,**	[Time (slope) + Solution (slope)/ Session nested within Mouse (intercept)] + [Bout nested in Session within Mouse (intercept)] + [Bout (intercept)]	Signal
Session (Lvl 3)	**Time** (Lvl 1)**, Solution** (EtOH, Water, Sucrose), Session-Level Characteristics: Consumption (mL/kg, g/kg)	[Mouse (intercept)]	Session-Level Drinking Characteristics
Bout (Lvl 2)	**Time** (Lvl 1), Bout-Level Characteristics: Bout Duration, Onset Time (Position)	[Session nested within Mouse (intercept)]	Bout-Level Drinking Characteristics
Time Around Bout (Lvl 1)	**Time** (Before, After)		

Figure 2. Experimental Data Structure

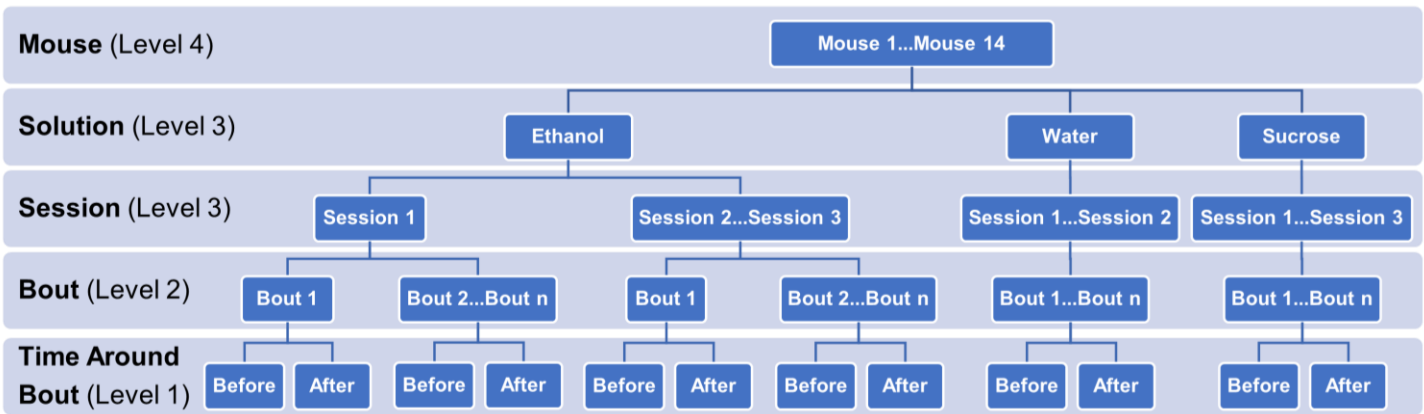

CeA^{Dyn} Calcium Transients Around Drinking

A priori, we were interested in the differences in calcium signal around a bout of drinking based on which solution was being consumed and the biological sex of the mouse. The average calcium signal within a 30 second window, before and after a drinking bout for EtOH, water, or sucrose is shown in **Figure 3**, and individual bout signals and group averages are shown in **Figure 4A**. To analyze this signal in more detail, we first fit a MLMM with Sex (Level 4), Solution (Level 3), and Time around bout (Level 1) as fixed factors with standardized calcium signal as the outcome variable and compared estimated means. Based on random effect optimization, we allowed the intercept to vary for each session within mouse, each bout within session and mouse, and each bout

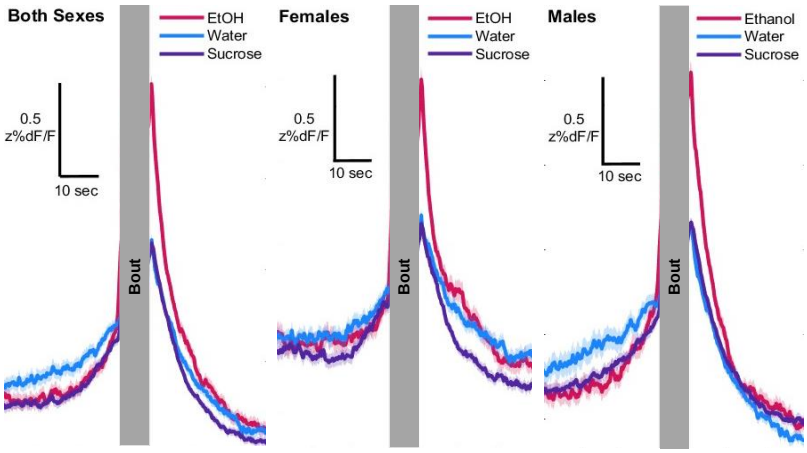

FIGURE 3. Average calcium activity traces for 20 sec before and after drinking bouts (grey region) for EtOH, water, or 0.5% sucrose. Traces are shown for all bouts (A), females (B), and males (C). Shaded regions around each line indicate standard error.

unnested due to bout being also crossed between mice and solutions. Since we had sufficient power with this outcome, in the final signal model, we also included a random slope for a Time and Solution slope with the Mouse:session intercept to adequately control for interactions between these lower-level variables with any higher level variable (Heisig and Schaeffer 2019). This model revealed that there were significant effects of Time such that signal after a bout was larger than signal before the bout (After-Before: 0.327 ± 0.028 z%dF/F (EM ± SE), $t_{43.53}$ = 11.746, p < 0.0001; **Fig 4A**) and an effect of Solution where the average signal for EtOH was higher than the average of water and sucrose jointly (EtOH–water/sucrose: 0.152 ± 0.042 z%dF/F (EM ± SE), $t_{39.89}$ = 3.611, p = 0.0008; **Fig 4A**). There was also a statistically significant interaction between Solution and Time around bout where EtOH had a larger change in signal after a drinking bout than sucrose and water drinking bouts jointly (EtOH change from Time–water/sucrose change from Time: 0.118 ± 0.008 z%dF/F (EM ± SE), t_{3161} = 14.060, p < 0.0001; **Fig 4A**). There were no other effects that were statistically significant (p > 0.1233), including the effect of Sex. The estimated means, collapsed across sex, and corresponding confidence intervals from this model are shown in **Figure 4B**.

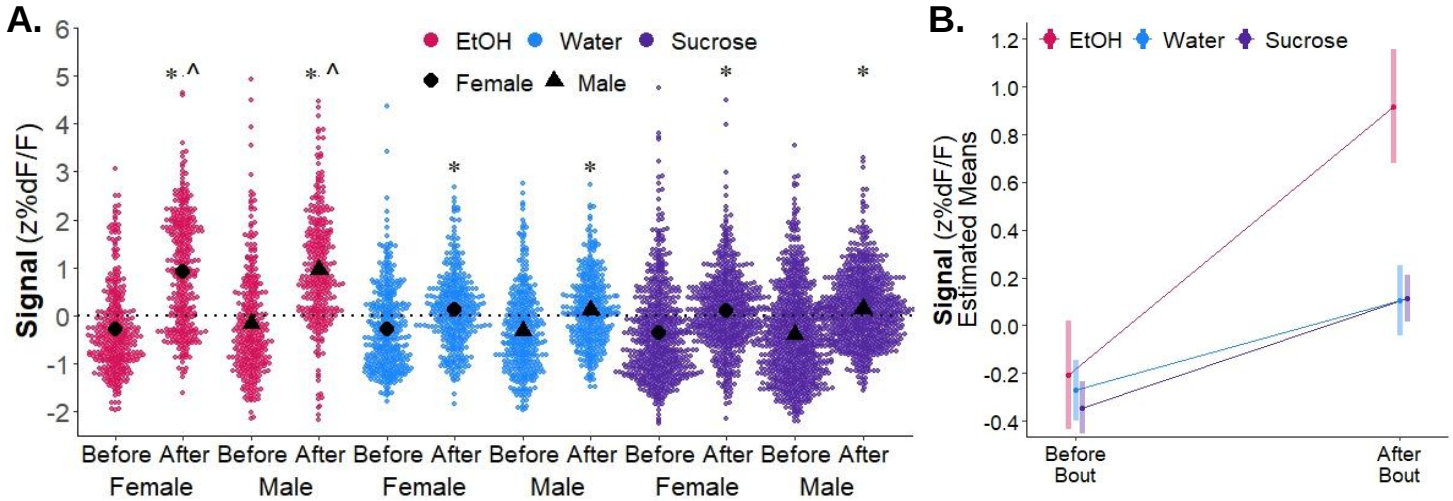

FIGURE 4. (A) Calcium signal before and after individual bouts for EtOH (red), water (blue), and 0.5% sucrose (purple) with group means indicated by black symbols (circles: female, triangles: males). (B) The signal-outcome MLMM indicated that there were no sex differences or interactions, thus estimated means and confidence intervals are shown, collapsed across sex. Signal after bouts were significantly higher than before bouts for all solutions (*, p < 0.05) but EtOH showed a statistically significant more pronounced increase in signal after the bout compared to water/sucrose jointly (^, *, p < 0.05).

Drinking Characteristic Differences

We next hypothesized that the calcium signal from these neurons may be associated with unique differences in drinking behavior for EtOH compared to water and sucrose. To test this hypothesis, we first characterized drinking behavior differences between the solutions with the intent of discovering candidate variables to include as predictors in the signal outcome model. Despite a lack of sex-dependent effects on signal from the previous analysis, sex nevertheless could have mediated relationships between drinking behavior and signal. Thus, we investigated the impact of both sex and solution on drinking characteristics using an outcome model for each drinking characteristic. We focused on the characteristics Bout Duration and onset time (Position) at the bout level (Level 2) and Consumption (mL/kg) at the session level (Level 3). For illustration purposes, individual session (**Figure 5**) or bout means (**Figures 6-7**) and group means ± standard error for drinking characteristics are displayed. At the session level, the amount of each solution consumed (in mL/kg, **Figure 5**), was associated with Sex and Solution in that females, on average, drank more than males (female-male: 4.998 ± 1.628 mL/kg (EM ± SE), $t_{12.10}$ = 3.069, p = 0.0097), sucrose consumption was higher than water (sucrose-water: 3.198 ± 1.130 mL/kg (EM ± SE), $t_{104.72}$ = 2.828, p = 0.0056), and EtOH was lower than sucrose and water jointly (EtOH-sucrose/water: -4.401 ± 0.630 mL/kg (EM ± SE), $t_{105.65}$ = -6.986, p < 0.0001). There was also an interaction of Sex and Solution where females drank much less EtOH than sucrose and water and this decrease was not as great in males (female Change from EtOH-male change from EtOH: 1.671 ± 0.630 mL/kg (EM ± SE), $t_{105.65}$ = 2.652, p = 0.0092). For EtOH specifically, there was no consumption difference between males and females (posthoc; female EtOH-male EtOH: 3.313 ± 4.067 mL/kg (EM ± SE), $t_{27.98}$ = 0.814, p = 0.9624). However, Sex differences between males and females were present for water and sucrose where females drank more than

males (posthoc; female-male water: 14.416 ± 4.430 mL/kg (EM ± SE), $t_{38.24}$ = 3.254, p = 0.0267; female-male sucrose: 12.258 ± 3.932 (EM ± SE), $t_{25.08}$ = 3.118, p = 0.0462). The estimated means for the Consumption model are shown in **Figure 5B** demonstrating that mice consumed less EtOH than water or sucrose.

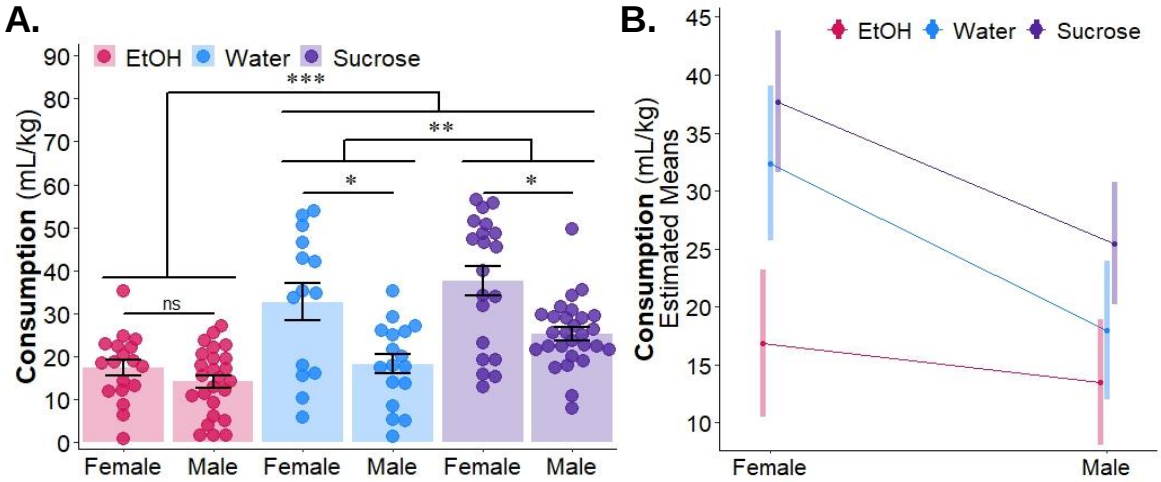

FIGURE 5. Consumption of each solution in mL/kg for each sex (A). MLMM for Consumption (B) showed that females generally drank more than males, except with EtOH where both sexes drank similar amounts, and both sexes drank more water than EtOH and more sucrose than both EtOH or water. ns, not significant; * ,p < 0.05; **, p < 0.001; ***, p < 0.0001.

At the bout level, Bout Duration (**Figure 6**) showed an effect of Sex where males had longer bout duration than females (male-female; 0.581 ± 0.135 sec (EM ± SE), $t_{38.05}$ = 4.310, p = 0.0001) and an effect of Solution where sucrose bouts were longer than water bouts (sucrose-water: 0.199 ± 0.061 (EM ± SE), t_{2548} = 3.278, p = 0.0011) and EtOH had longer bout durations than water and sucrose jointly (EtOH-water/sucrose: 0.383 ± 0.039 (EM ± SE), t_{2643} = 9.861, p< 0.0001). There was also a significant interaction between the effect of Sex and Solution, where males exhibited longer EtOH bout duration compared to water/sucrose than females (male EtOH change from water/sucrose-female EtOH change from water/sucrose: 0.117 ± 0.039 sec (EM ± SE), t_{2643} = 2.999, p = 0.0027). Within EtOH and sucrose but not water, males drank in longer bouts than females (posthoc; male EtOH-female EtOH: 1.627 ± 0.319 sec (EM ± SE), $t_{103.70}$ = 5.108, p < 0.0001; male sucrose-female sucrose: 0.965 ± 0.286 (EM ± SE), $t_{68.71}$ = 3.370, p = 0.0150; male water-female water: 0.892 ± 0.317 (EM ± SE), $t_{100.32}$ = 2.811, p = 0.0639). The estimated means for the Bout Duration model are shown in **Figure 6B**. Altogether, these results suggested that under these conditions mice drink EtOH in uniquely longer bouts than water and sucrose and that males and females drink EtOH in different length bouts, despite consuming similar EtOH amounts at the session level.

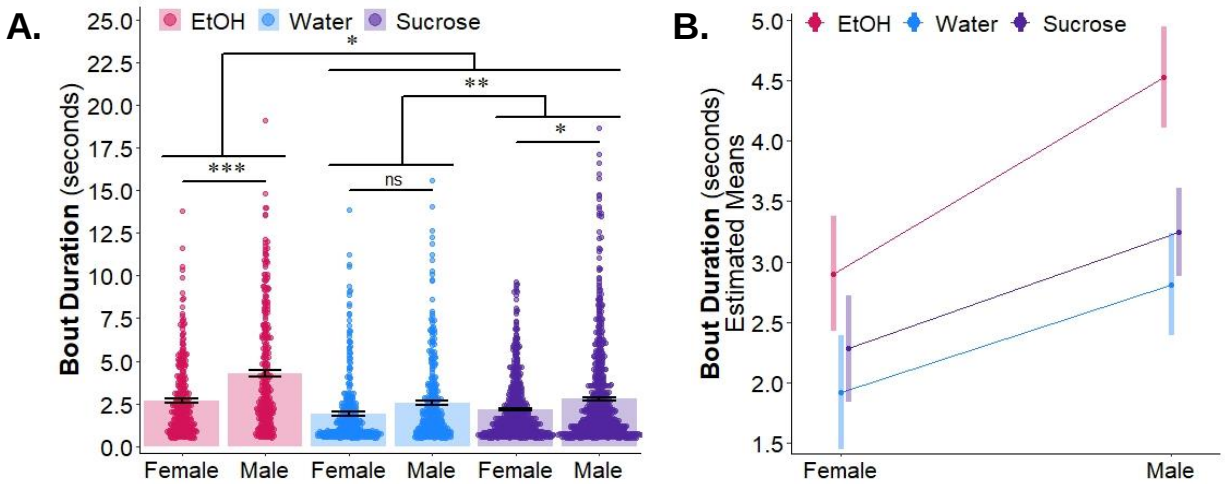

FIGURE 6. Bout Duration of each bout by sex and solution (A). MLMM for Bout Duration (B) indicated that both sexes have longer bout durations for EtOH and that within EtOH, males had longer bout durations than females. *, p< 0.05; p < 0.001; ***, p < 0.0001.

Signal-Characteristic Relationships

Since the unique signal change around an EtOH drinking bout might be explained by EtOH's lower session consumption, we investigated whether lower consumption of solutions led to a larger increase in signal due to Time. To test this, we constructed an individual mouse mean-centered consumption variable (scaled and centered around mouse-specific overall mean consumption to account for individual differences) and included this as a predictor in the signal-outcome model. Including consumption amount (low, mean, high) in the model only modestly changed the previous effects of Time (EM 0.327 > 0.311), EtOH (0.152 > 0.139), and change in EtOH signal due to Time (0.118 > 0.115) even though model fit was significantly increased (Log Likelihood Test, χ^2_{12} = 35.329, p = 0.0004). This indicated that consumption amount does not predominantly explain previous effects. Adding consumption to the model also introduced new interactions with Sex (**Figure 7**). There was no effect of higher consumption on signal by itself (-0.025 ± 0.046 z%dF/F (EM ± SE), $t_{65.06}$ = -0.558, p = 0.5787) but, on average, higher EtOH consumption specifically led to a slightly lesser increase in signal due to Time in males (male high EtOH-drinking change from Time-female high EtOH-drinking change from Time: -0.027 ± 0.012 z%dF/F (EM ± SE), t_{1613} = -2.259, p = 0.0240). This model suggested that males and females have opposite changes in estimated signal means during a session of higher EtOH consumption relative to their own overall consumption mean. Consumption did not appreciably mediate signal change from Time for sucrose. During high drinking water sessions, water no longer showed an effect of Time in either sex (posthoc; male water after-before bout: 0.016 ± 0.145 (EM ± SE), $t_{408.35}$ = 0.110, p =1; female water after-before bout: 0.325 ± 0.123 (EM ± SE), $t_{179.35}$ = 2.641, p = 0.2651). The implication of these results is that amount of consumption does not explain greater activity of CeA^{Dyn} neurons for EtOH.

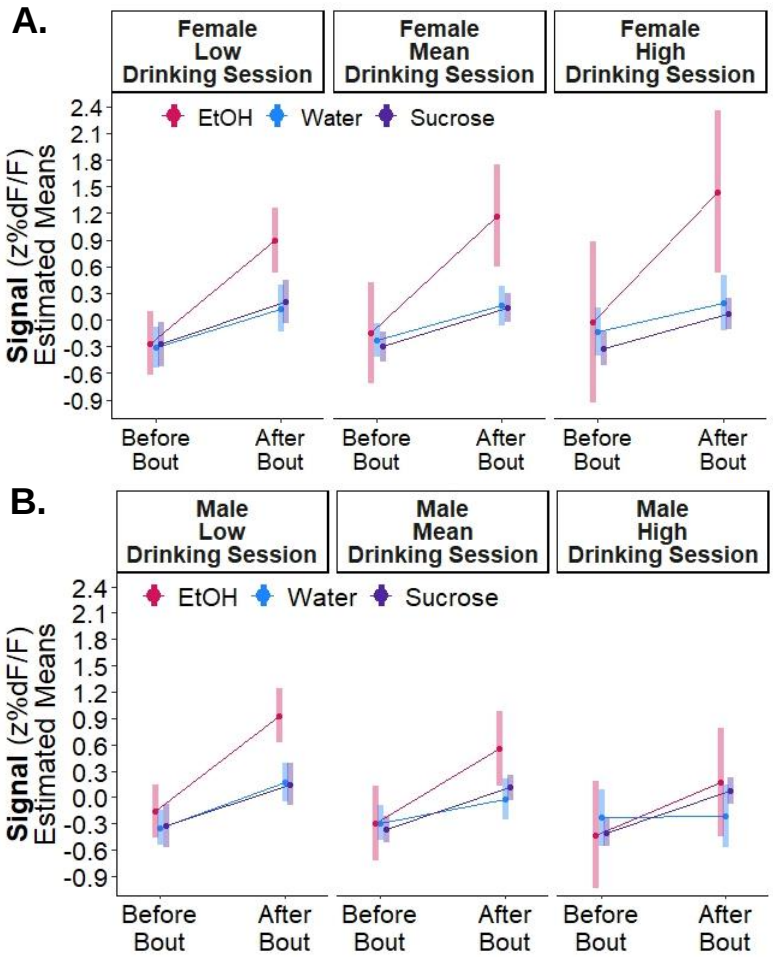

FIGURE 7. MLMM estimated means for individual consumption effects on calcium signal in females (A) or males (B) during sessions with low, average, or high consumption. Sexes show opposite effects of consumption where females show an increase in signal during high drinking sessions whereas males show a decrease in signal during high drinking sessions.

Next, since each solution also showed differences in bout-level characteristics, we first investigated the relationship between signal and bout duration. We expected that bout duration would show a stronger relationship with momentary signal around a bout of drinking. When individually scaled and centered Bout Duration was added to the signal outcome model, the effects of Time (EM 0.327>0.317) and change in EtOH signal due to Time (0.118>0.095) decreased slightly while the effect of EtOH remained identical (0.152>0.152) even though model fit was significantly increased (Log Likelihood Test, χ^2_{12} = 187.046, p < 0.0001). This indicated that Bout Duration also did not explain the elevated GCaMP7 signal for EtOH, while having a relationship to signal nonetheless. There was not a statistically significant effect of Bout Duration alone on signal (p = 0.7410) but this variable interacted with the effects of Time and Sex individually such that signal change due to Time was higher with longer durations compared to a mouse's mean (effect of Time with longer durations – effect of Time with shorter durations: 0.130 ± 0.011 z%dF/F (EM ± SE), t_{3543} = 12.296, p < 0.0001) and when males drank longer than usual, this slightly decreased signal (male effect of higher duration-female effect of higher duration: -0.068 ± 0.013 z%dF/F (EM ± SE), t_{5124} = -5.165, p < 0.0001). There was also an interaction with sucrose such that there was a small decrease in the effect of Time for sucrose compared to water (water effect of Time-sucrose effect of Time: 0.045 ± 0.013 z%dF/F (EM ± SE), t_{3537} = 3.445, p = 0.0006)

and an interaction of this effect with Sex where signal was even lower in males (male-female effect of Time with longer duration difference between sucrose and water: -0.027 ± 0.013 z%dF/F (EM ± SE), t_{3537} = -2.037, p = 0.0417). Further examining the estimated means plot for each Sex as a function of Bout Duration (**Figures 8A-B**), this complex interaction can be summarized as follows: the change in signal from pre- to post-bout increases for all solutions as an animal drinks longer than they usually do, but that water increases more relative to sucrose and does so more in males than females. These results, when combined with the previous results indicating that both sexes showed the longest bout durations with EtOH, then sucrose, then water seems to suggest that the signal gains for drinking longer than usual for water are more than those for EtOH and sucrose. This relationship becomes more evident when these estimated means are collapsed across Sex (**Figure 8C**). It is clear from these results that bout duration has a relationship with signal, albeit complex, but that this relationship still cannot explain EtOH's unique engagement of CeA^{Dyn} neurons.

Finally, we were interested whether the temporal occurrence of the bout within the 2-hr session was predictive of signal and if the signal changed as a response to satiation. To do so, we added 'Position' within the session to the signal outcome model. Our hypothesis was that EtOH would show a uniquely higher initial increase that would habituate over the 2-hr drinking sessions. Including Position in the signal outcome model significantly increased model fit (Log Likelihood Test, χ^2_{24} = 83.031, p < 0.0001). The estimated means for the signal for bouts within first and last 10 min and the time in between are shown in **Figure 9**. There was a small but statistically significant effect of Position alone where the signal overall within the first 10 min was higher than the rest of the session (First 10 min-rest of session: 0.045 ± 0.019 (EM ± SE), t_{1477} = 2.360, p = 0.0184). When Position was introduced to the model, there was an effect of Sex (males-females: 0.089 ± 0.044 (EM ± SE), $t_{82.84}$ = 2.031, p = 0.0454), but no interactions with Sex (**Figure 9**). Surprisingly, there was an effect of the first 10 minutes with sucrose signal relative to the mean of the rest of the session, irrespective of Time (sucrose first 10 min-water first 10 min: 0.064 ± 0.020 (EM ± SE), t_{4405} = 3.119, p = 0.0018). Further, since there was no interaction of Position with the change in EtOH signal due to Time, this signal not habituate across the 2-hr session (EtOH signal change vs water/sucrose signal first 10 min-EtOH signal change vs water/sucrose signal rest of the session: 0.011 ± 0.010 (EM ± SE), t_{3554} = 1.090, p = 0.2758). Again, as with total consumption within a session and bout duration, temporal occurrence of the bout was related to signal but also did not explain the unique signal for EtOH.

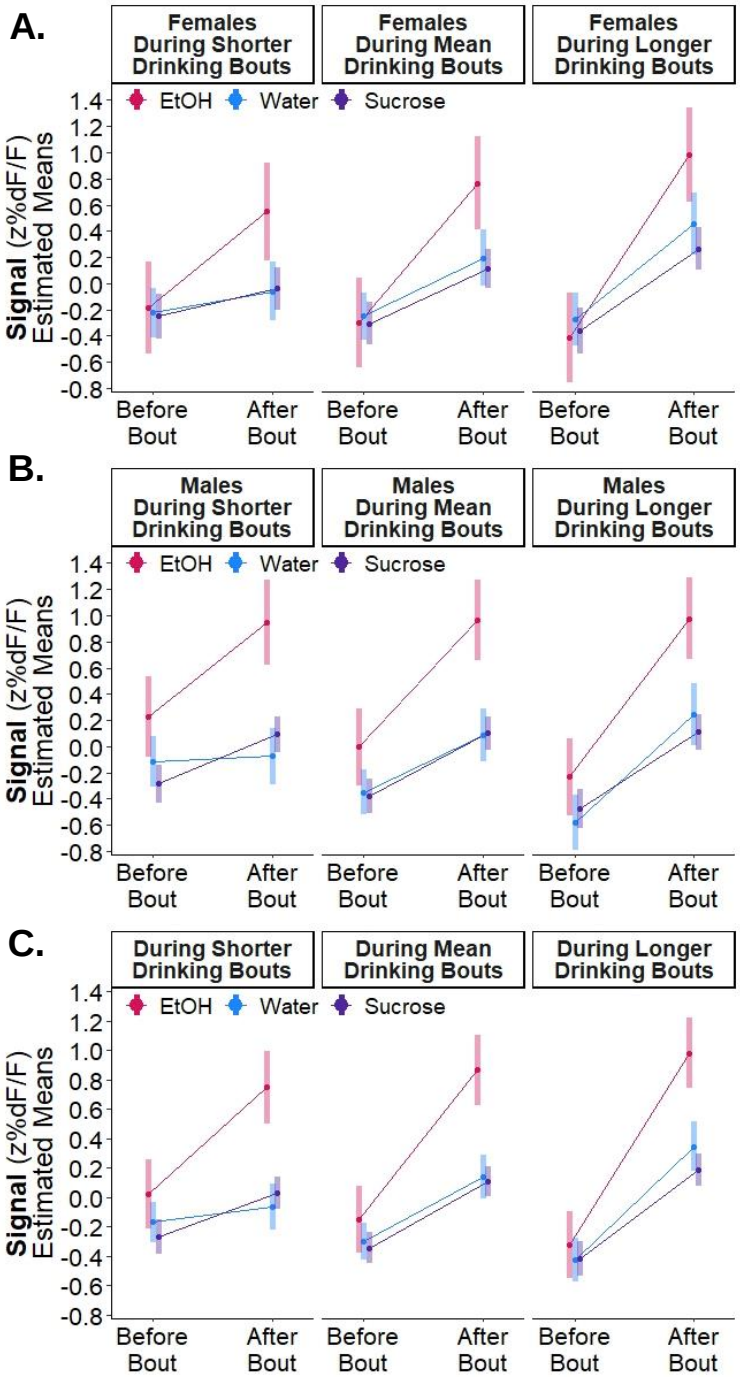

FIGURE 8. Estimated means for bout duration in (A) females, (B) males, and (C) collapsed across sex.

Discussion

Dynorphin-expressing neurons in the central amygdala (CeA^{Dyn}) have been heavily implicated in mediating binge alcohol intake and excessive alcohol drinking produced by the interaction of stress and alcohol dependence.

The current fiber photometry study demonstrated that EtOH drinking uniquely engages the CeA^{Dyn} neuronal population – there is higher activity in CeA^{Dyn} neurons after a bout of drinking alcohol than after drinking water and sucrose. Our analysis tested whether unique drinking characteristics for alcohol relative to water and sucrose explain this unique alcohol-evoked signal. While these drinking characteristics modulated the signal, none satisfactorily explain alcohol 's greater engagement of CeA^{Dyn} neurons. We speculate that there is a unique physiological action of alcohol that evokes increased activity in CeA^{Dyn} neurons and propose that understanding this relationship will clarify interactions between behavior shown to rely on CeA^{Dyn} neuronal activity, like stress or defensive responses, and long-term alcohol exposure.

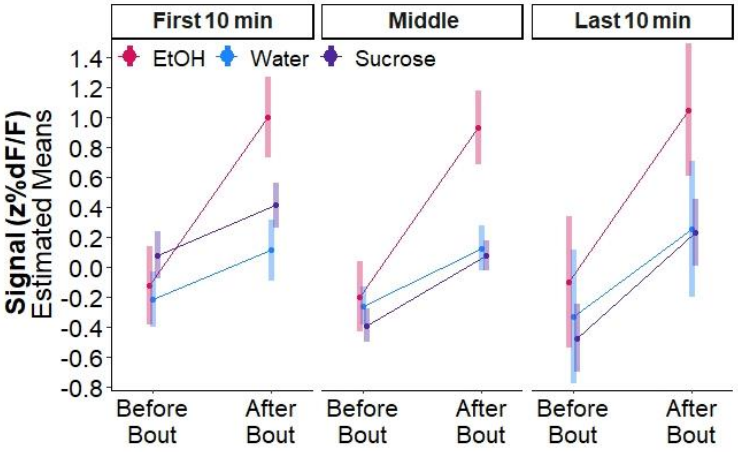

Figure 9. Estimated means showing effect of temporal occurrence on signal

That alcohol evokes greater increased activity in CeA^{Dyn} neurons than what is evoked by water or sucrose has important implications for the role of these neurons in alcohol drinking and on alcohol effects on behavior governed by the CeA^{Dyn} population. Importantly, the increased magnitude of calcium transients was present when mice consumed alcohol for the first time (data not shown). This suggests that alcohol innately engages these neurons in an unique manner even prior to experiencing its intoxicating effects. This raises questions about the evolutionary purpose of such a response and the possibility that there is a sensory explanation for the distinct response to alcohol. Alcohol, but not water nor sucrose, causes chemesthetic sensations like burning, tingling, and drying, which in humans is negatively associated with frequency of alcohol drinking (Nolden and Hayes 2015). These chemesthetic sensations are thought to help protect animals from environmental irritants or toxins in the case olfaction does not provide sufficient cues (see Green 2012). Future studies can test this possibility by measuring in vivo activity of these neurons while manipulating the concentration of alcohol to change the profile of these chemesthetic sensations. In this role, we predict that neural adaptations would occur with more chronic activation of CeA^{Dyn} neurons by alcohol. However, instead of these neurons becoming less responsive, previous work shows that repeated alcohol exposure increases excitability of CeA^{Dyn} neurons, though this effect was sex-specific (males only) and derived from ex vivo electrophysiology. Future studies can test the impact of long-term alcohol drinking and alcohol dependence on these neurons in both sexes in vivo to better understand CeA^{Dyn} neuron adaptations that contribute to AUD-related behavioral phenotypes.

Another possibility is that the unique alcohol-evoked activity in CeA^{Dyn} neurons reflects a response to the distinct taste characteristics of alcohol relative to water and sucrose. Alcohol is reported to exhibit both bitter and sweet tastes in humans, with bitter taste dominating at lower alcohol concentrations (≤16%; Nolden and Hayes 2015). Though we cannot assess the subjective experience of taste in mice directly, one study cleverly used stimulus generalization after conditioned taste aversion to examine which taste is perceptually most similar to alcohol (Blizard 2005). They reported that both quinine and sucrose taste aversion generalize to alcohol and vice versa. While we do not see a similar increase in signal around a bout of drinking sucrose as alcohol here, we only tested one concentration of sucrose, which may not be perceptually similar in sweetness as 15% alcohol. The study described used many orders of magnitude more concentrated sucrose (200 mM or 6.8%) than the current study. To capture whether the bitter taste component of alcohol is what produces the unique CeA^{Dyn} activity, future studies should measure CeA^{Dyn} activity during consumption of varying concentrations of quinine or, perhaps even more relevant, mixtures of sucrose and quinine that are proposed to better mimic the taste of alcohol (see Mukherjee et al 2023).

A third possible explanation of alcohol drinking's unique evocation of CeA^{Dyn} activity is that this activity encodes innate alcohol reinforcement, which could lead to excessive alcohol intake with repeated exposure. While this explanation might be attractive because it suggests alcohol's reinforcement is "hard-wired", there is a great discussion in Janiak et al (2020) that suggests that higher alcohol metabolism evolves in animals that have a greater fruit and nectar component of their diet to help counter intoxication from consumption of fermented fruits. In this light, the well-documented high alcohol metabolism of *Mus musculus* suggests that this species evolved

to deal with alcohol and counter intoxication because of a high fruit diet. Thus, any reinforcement signal evoked by alcohol may better reflect the co-occurrence of alcohol with highly palatable fruits. This is of course purely speculative and would need to be empirically tested.

Recently, others have also investigated CeA^{Dyn} neuron activity around alcohol consumption and found that water, sucrose, and alcohol equally evoked CeA^{Dyn} neuronal activity after a drinking bout (Roland et al, preprint). While potentially at odds with our findings, there are methodological differences that could account for the differing results. Firstly, mice were water deprived in Roland et al to encourage drinking during short test periods, whereas our mice were not. While the authors mention they tested the same mice in water non-deprivation states and saw no differences in mean Z-scored signals for water or alcohol in the CeA, it is unclear whether water deprivation would specifically influence signal in the CeA^{Dyn} subpopulation, which showed several notable differences in dynamics than the pan CeA recordings in their study (e.g. habituation, sex differences). Future studies should more systematically test the effects of deprivation state on evoked CeA^{Dyn} activity to address this aspect. We also allowed 2-hr for drinking instead of 5 second window per solution. This manipulation could change the urgency/motivation to respond and modify alcohol-water signal differences after a bout. While the bulk of the bout durations were below 5 seconds for each solution, there were a significant number of much longer bouts (~10-15 seconds) in our study when mice were allowed to voluntarily choose when and how long to drink. Secondly, during each of our 2-hr sessions, mice were only allowed access to a single testing solution, whereas in Roland et al, mice would get access to multiple solutions in sequence because the analysis window was shorter. It is unclear what impact the novelty or salience of always receiving a new solution would have on relative evoked signals. They also tested a 10-fold higher concentration of sucrose (5% vs 0.5%) which could have an impact on bout-induced CeA^{Dyn} activity to reduce signal differences between sucrose and alcohol and indeed, taste of sucrose concentrations around 5% (6.8%) may better generalize to alcohol solutions based on previous studies (Blizard 2005). The different concentrations of alcohol used between our studies (15% vs 20%) may also have impacted these relative signal differences and taste profiles. Future studies should investigate the effects of altering the concentrations of solutions on the resulting relative post-bout neural activity. Despite these differences, both studies' results agree that CeA^{Dyn} activity increases from a bout of alcohol drinking and does not habituate over time.

In summary, alcohol drinking resulted in a uniquely large increase in CeA^{Dyn} activity in both male and female mice. While drinking characteristics had a moderating influence on the magnitude of the increase in signal for alcohol relative to water and sucrose, none satisfactorily explained the unique alcohol-evoked CeA^{Dyn} activity. The unique engagement of the CeA^{Dyn} neuron population for alcohol could have important implications for alcohol influences on stress and appetitive behavior governed by the CeA. Thus, it is necessary to study CeA^{Dyn} neurons as a potential crucial cell population to explain behavioral adaptations observed in models of alcohol dependence.

References

Aarts, E., Verhage, M., Veenvliet, J. V., Dolan, C. V. & Sluis, S. van der. A solution to dependency: using multilevel analysis to accommodate nested data. *Nat. Neurosci.* 17, 491–496 (2014).

Anderson, R. I. et al. Dynorphin-kappa opioid receptor activity in the central amygdala modulates binge-like alcohol drinking in mice. Neuropsychopharmacology : official publication of the American College of Neuropsychopharmacology 44, 1084–1092 (2019).

Blizard, D. A. Sweet and Bitter Taste of Ethanol in C57BL/6J and DBA2/J Mouse Strains. Behav Genet 37, 146 (2006).

Bloodgood, D. W. et al. Kappa opioid receptor and dynorphin signaling in the central amygdala regulates alcohol intake. Molecular psychiatry (2020) doi:10.1038/s41380-020-0690-z.

Bohnslav, J. P. et al. DeepEthogram, a machine learning pipeline for supervised behavior classification from raw pixels. eLife 10, e63377 (2021).

Boor, C. de. On calculating with B-splines. J. Approx. Theory 6, 50–62 (1972).

Boughter, J. D., Baird, J. -P., Bryant, J., John, S. J. St. & Heck, D. C57BL/6J and DBA/2J mice vary in lick rate and ingestive microstructure. Genes, Brain Behav. 6, 619–627 (2007).

Davis, J. D. & Smith, G. P. Analysis of the Microstructure of the Rhythmic Tongue Movements of Rats Ingesting Maltose and Sucrose Solutions. Behav. Neurosci. 106, 217–228 (1992).

Eilers, P. H. C. & Marx, B. D. Flexible smoothing with B-splines and penalties. Stat. Sci. 11, (1996).

Gueorguieva, R. & Krystal, J. H. Move Over ANOVA: Progress in Analyzing Repeated-Measures Data andIts Reflection in Papers Published in the Archives of General Psychiatry. *Arch. Gen. Psychiatry* 61, 310–317 (2004).

Hastie, Trevor, et al. The elements of statistical learning: data mining, inference, and prediction. Vol. 2. New York: springer, 2009.

Haun HL, Lebonville CL, Solomon MG, Griffin WC, Lopez MF, Becker HC. 2022. Dynorphin/Kappa Opioid Receptor Activity Within the Extended Amygdala Contributes to Stress-Enhanced Alcohol Drinking in Mice. Biol Psychiat. doi:10.1016/j.biopsych.2022.01.002

Heisig, J. P. & Schaeffer, M. Why You Should Always Include a Random Slope for the Lower-Level Variable Involved in a Cross-Level Interaction. *Eur. Sociol. Rev.* 35, 258–279 (2019).

Johnson, A. W. et al. An analysis of licking microstructure in three strains of mice. Appetite 54, 320–330 (2010).

Mukherjee, A. et al. Escalation of alcohol intake is associated with regionally decreased insular cortex activity but not changes in taste quality. Alcohol Clin Exp Res (2023) doi:10.1111/acer.15060.

Nolden AA, Hayes JE (2015) Perceptual Qualities of Ethanol Depend on Concentration, and Variation in These Percepts Associates with Drinking Frequency. Chemosens Percept 8:149–157.

Rinker, J. A. et al. Prelimbic neuron calcium activity predicts perceived hedonic value across drinking solutions and ethanol dependent states in mice. bioRxiv 2023.04.04.535635 (2023) doi:10.1101/2023.04.04.535635.

Roberto, M., Kirson, D. & Khom, S. The Role of the Central Amygdala in Alcohol Dependence. Csh Perspect Med 11, a039339 (2020).

Roland, A.V., Chao, T.-H.H., Hon, O.J., Machinski, S.N., Sides, T.R., Lee, S.I., Shih, Y.-Y.I., and Kash, T.L. (2023). Acute and chronic alcohol modulation of extended amygdala calcium dynamics. bioRxiv, 2023.10.10.561741. 10.1101/2023.10.10.561741.

Sacks JJ, Gonzales KR, Bouchery EE, Tomedi LE, Brewer RD. 2010 national and state costs of excessive alcohol consumption. Am J Prev Med. 2015;49(5):e73-e79. PubMed PMID: 26477807

SAMHSA, Center for Behavioral Health Statistics and Quality. 2022 National Survey on Drug Use and Health. Table 5.9A—Alcohol use disorder in past year: among people aged 12 or older; by age group and demographic

characteristics, numbers in thousands, 2021 and 2022. [cited 2023 Dec 8]. Available from: https://www.samhsa.gov/data/sites/default/files/reports/rpt42728/NSDUHDetailedTabs2022/NSDUHDetailedTabs2022/NSDUHDetTabsSect5pe2022.htm#tab5.9a

Walker, L. C. A balancing act: the role of pro- and anti-stress peptides within the central amygdala in anxiety and alcohol use disorders. J Neurochem 157, 1615–1643 (2021).

West, B. T., Welch, K. B., Gałecki, A. T. & Gillespie, B. W. Linear Mixed Models, A Practical Guide Using Statistical Software. (2022) doi:10.1201/9781003181064.

WHO. Global status report on alcohol and health 2018. Geneva, Switzerland: WHO Press; 2018 [cited 2022 Apr 27], p. vii. Available from: https://www.who.int/publications/i/item/9789241565639

Yaremych, H. E., Preacher, K. J. & Hedeker, D. Centering Categorical Predictors in Multilevel Models: Best Practices and Interpretation. *Psychol. Methods* 28, 613–630 (2021).